

# **Bursty Bulk Flow Turbulence as a Source of Energetic Particles to the Outer Radiation Belt**

R. E. Ergun<sup>1,2</sup>, M. E. Usanova<sup>2</sup>, D. L. Turner<sup>3</sup>, and J. E. Stawarz<sup>4</sup>

---

Corresponding author: Robert E. Ergun, Laboratory of Atmospheric and Space Sciences,  
University of Colorado, Boulder, Colorado, USA 80303. ree@lasp.colorado.edu.

<sup>1</sup> Department of Astrophysical and Planetary Sciences, University of Colorado, Boulder, Colorado, USA.

<sup>2</sup> Laboratory for Atmospheric and Space Physics, University of Colorado, Boulder, Colorado, USA.

<sup>3</sup> Johns Hopkins University Applied Physics Laboratory, Laurel, MD, USA

<sup>4</sup> The Blackett Laboratory, Imperial College London, United Kingdom

## **Key Points:**

Observations of a bursty bulk flow penetrating to  $\sim 7 R_E$  display turbulent electric fields accompanied by enhanced energetic ions and electrons.

Ions and electrons appear to be locally accelerated by turbulent electric fields.

Turbulent electric fields in the BBF breaking region favors energization of the highest energy electrons, which leads to acceleration.

## Abstract

We report observations of a Bursty Bulk Flow (BBF) penetrating to the outer edge of the radiation belt. The turbulent BBF braking region is characterized by ion velocity fluctuations, magnetic field ( $\mathbf{B}$ ) variations, and intense electric fields ( $\mathbf{E}$ ). In this event, energetic ( $>100$  keV) electron and ion fluxes are appreciably enhanced. Importantly, fluctuations in energetic electrons and ions suggest that they are locally energized. Using correlation distances and other observed characteristics of turbulent  $\mathbf{E}$ , test-particle simulations support that local energization by  $\mathbf{E}$  favors higher-energy electrons and leads to an enhanced energetic shoulder and tail in the electron distributions. The energetic shoulder and tail can be amplified to MeV energies by adiabatic transport into the radiation belt where  $|\mathbf{B}|$  is higher. This analysis suggests that turbulence generated by BBFs can, in part, supply energetic particles to the outer radiation belt and that turbulence can be a significant contributor to particle acceleration.

## 1. Introduction

Turbulence, by its very nature, cascades energy in a driven system to smaller scales at which dissipation takes place. In Earth's magnetotail, the energy source is often magnetic field ( $\mathbf{B}$ ) annihilation enabled by magnetic reconnection or the associated ion jet ( $V_{Ion}$ ) and Poynting flux. As energy stored in  $\mathbf{B}$  and  $V_{Ion}$  cascades to smaller scales, the electric field ( $\mathbf{E}$ ) follows suit to carry out the transfer of  $\mathbf{B}$  and  $V_{Ion}$  energy into thermal energy. We hypothesize that, for electrons in a magnetized plasma, those with the highest energies have the largest gyroradii and largest parallel velocities, so they receive energy from large-scale and small-scale  $\mathbf{E}$  fluctuations. Particles with the lowest energies are last in line as they receive energy only from the smallest scales of  $\mathbf{E}$ . As a result, turbulent energization favors energetic particles, which results in acceleration.

In this letter, we concentrate on electron energization on closed field lines in the turbulent environment created by Bursty Bulk Flows (BBFs, Baumjohann et al., 1989; Angelopoulos et al., 1992; 1994). BBFs account for a significant fraction of energy transport from the Earth's magnetotail to the outer radiation belt and plasmasphere and likely lead to aurora (e.g., Sergeev et al., 1999; 2000; Nakamura et al., 2001; Sergeev et al., 2014; Ergun et al., 2015; Stawarz et al., 2015; Turner et al., 2015; 2016; 2021). They usually originate in the magnetotail beyond  $\sim 15 R_E$  (Earth radius) by magnetic reconnection events that are localized in the GSE  $Y$  (Geocentric Solar Ecliptic) direction (Ohtani, Singer, and Mukai, 2006; Runov et al., 2009; 2011; Sitnov, Swisdak, and Divin, 2009). BBFs often are accompanied by "dipolarization" in which stretched  $\mathbf{B}$  in the magnetotail (dominated by its GSE  $X$  component) relaxes to a more dipole-like configuration (GSE  $Z$  component increases). Dipolarization supports the hypothesis that BBFs are earthward-

flowing magnetic reconnection exhaust (e.g., Sitnov, Swisdak, and Divin, 2009; Nakamura, et al. 2009).

The characteristics of BBFs at distances more than  $\sim 8 R_E$  from Earth are fairly well described. At distances greater than  $\sim 12 R_E$ , Earthward flow velocities can reach up to  $1000 \text{ km s}^{-1}$  (Angelopoulos et al., 1992; 1994) and carry ram energy flux and Poynting flux (Stawarz et al., 2015). Flow velocities slow to the order of  $100 \text{ km s}^{-1}$  as BBFs travel from  $\sim 12 R_E$  to  $\sim 8 R_E$  due to stronger  $\mathbf{B}$  and higher densities. This region, called the BBF braking region, often displays strong turbulence, which energizes ions and electrons and launches Alfvén waves towards Earth’s ionosphere.

Properties of BBFs are less well understood inside of  $\sim 8 R_E$ . One of the key unknowns is how BBFs are related to enhancements of energetic particles in the outer radiation belts known as flow injections. Inside of  $\sim 8 R_E$ , the flows speeds of the progenitor BBFs are dramatically reduced and dipolarization is more difficult to identify in the strong  $\mathbf{B}$  environment, so correlation between BBFs and flow injections is challenging (Takada et al, 2006; Ohtani, Singer, and Mukai, 2006; Dubyagin et al, 2011, Sergeev et al., 2012; Liu et al., 2016).

Observations show that a subset of particularly strong BBFs generate turbulence in the braking region with intense  $\mathbf{E}$  (Ergun et al., 2015). Fluctuations in electron temperature ( $T_e$ ), ion temperature ( $T_i$ ), and in energetic fluxes are suggestive of local energization (Usanova and Ergun, 2022). Here, we investigate processes by which electrons are energized in a BBF that penetrates to the outer edge of the radiation belt. The Magnetospheric Multiscale (MMS) mission (Burch et al., 2016) has four satellites that, at the time, are separated by distances ranging from  $\sim 39$  to  $\sim 123 \text{ km}$ , which allows us to determine properties of the turbulent  $\mathbf{E}$  including a constraint on the correlation distances.

In this article, the term “energization” implies generic energy input to a species, “heating” is a thermal process in the core of a distribution, and “acceleration” is the development of a non-thermal tail. Particle energization is expected in the turbulent BBF braking region. However, a critical aspect is how the energy is distributed within the electron and ion distributions. Core heating results in an increase in  $T_i$  and  $T_e$ . If energization favors energetic particles, non-thermal distributions develop. Here, we show that the observed properties of  $\mathbf{E}$  result in non-thermal electron distributions that may seed the radiation belts.

## 2. Observations

Figure 1 displays a BBF penetrating to  $\sim 7 R_E$  from Earth’s center. The data are from the MMS satellites, which are, in this event, located in the southern magnetosphere. Figure 1a displays  $\mathbf{B}$  in GSE coordinates for a 50-minute period. The colors represent direction. The black trace is  $|\mathbf{B}|$ . Immediately below, panel b plots  $\mathbf{B}$  10-s detrended,  $d\mathbf{B} = \mathbf{B} - \langle \mathbf{B} \rangle_{10s}$ , which accentuates fluctuations in  $\mathbf{B}$ . Panels c, d, e, and f plot, respectively, ion flux as a function of energy from 70 to 600 keV, differential ion energy flux from 3 eV to 25 keV, electron flux from 60 to 500 keV, and differential electron energy flux from 6 eV to 25 keV. The MMS instruments are described in a series of articles (Torbert et al., 2016, Russell et al., 2016; Le Contel et al., 2016; Lindqvist et al., 2016, Ergun et al., 2016; Mauk et al., 2016; Pollock et al., 2016).

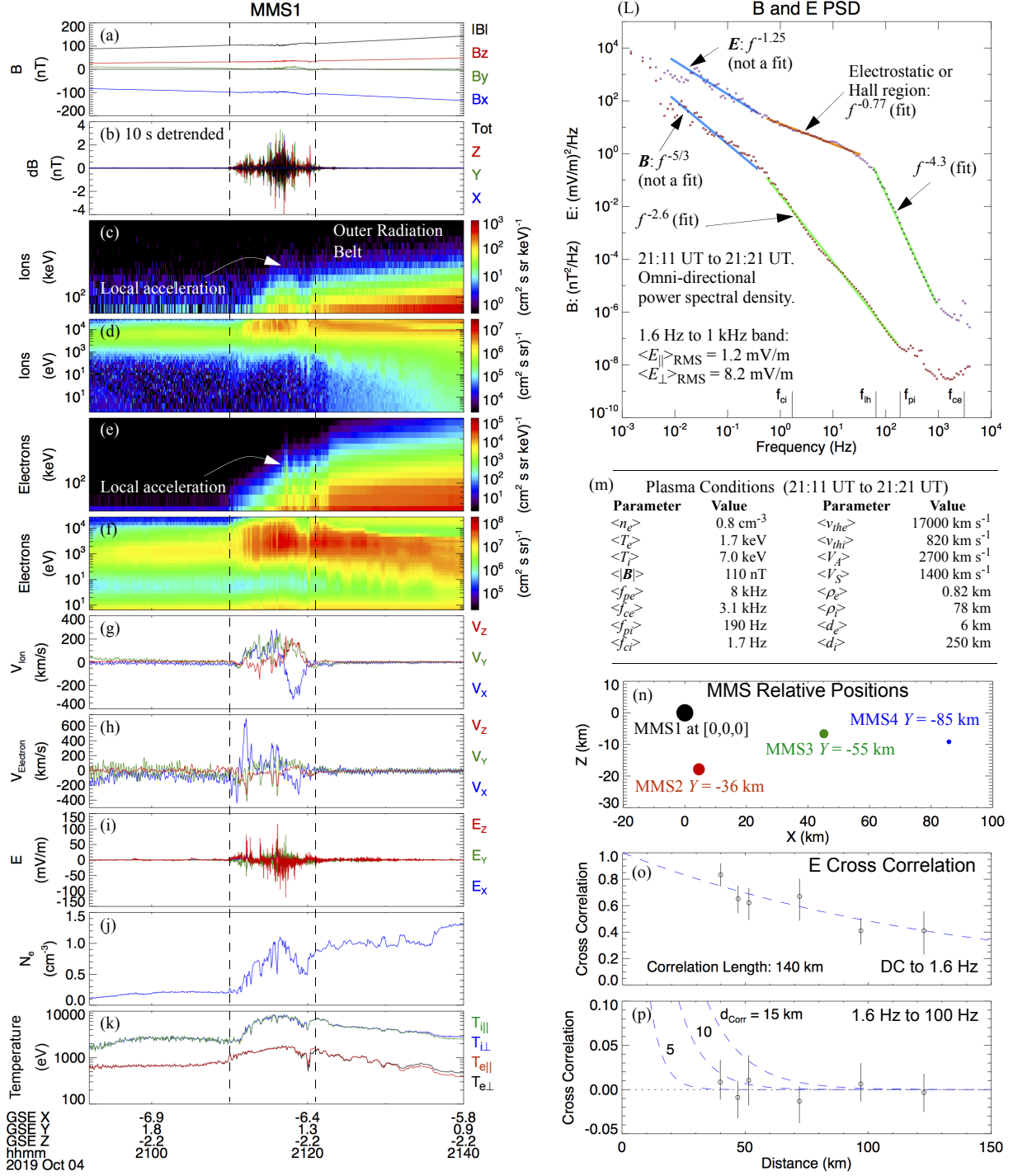


**Figure 1.** MMS1 observations of a BBF penetrating close to the outer radiation belt. The horizontal axis on the right column is 50 minutes in time. Vectors are in GSE coordinates; colors represent components as marked on the right of a panel. (a)  $B$  at 62.5 ms resolution. The

---

black trace is  $|\mathbf{B}|$ . (b)  $\mathbf{B}$  detrended by 10 s. (c) Ion flux as a function of energy (vertical axis) from 70 to 600 keV. These data are from all four MMS spacecraft. (d) Differential ion energy flux as a function of energy from 3 eV to 25 keV. (e) Electron flux from 60 to 500 keV. (f) Differential electron energy flux 6 eV to 25 keV. (g)  $V_{Ion}$  at 4.5 s resolution. (h)  $V_{Elc}$  at 4.5 s resolution smoothed over 13.5 s. (i)  $\mathbf{E}$  at 31.25 ms resolution. (j) Electron density at 4.5 s resolution. (k)  $T_i$  and  $T_e$  at 4.5 s resolution. (L) The PSD of  $\mathbf{B}$  and  $\mathbf{E}$  versus frequency. (m) Average plasma conditions. (n) The relative positions of the MMS spacecraft. (o) The cross-correlation of  $\mathbf{E}$  between the MMS spacecraft plotted as a function of separation.  $\mathbf{E}$  is filtered from DC to 1.6 Hz. (p) The cross-correlation of  $\mathbf{E}$  filtered from 1.6 Hz to 100 Hz.

---

At the beginning of Figure 1, ~20:50 UT, the MMS satellites are in a relatively quiet region of the magnetotail. The noticeable event begins at ~20:10 UT and endures until ~21:21 UT. During this period,  $\mathbf{B}$  has visible fluctuations (Figure 1b) and there is an enhancement of energetic (>100 keV) ion and electron fluxes (panels c-f). Importantly, the energetic fluxes are varying, which suggests local acceleration. At the same time,  $V_{Ion}$  (Figure 1g) indicates disturbed flow up to 200 km/s including a flow vortex (Birn et al., 1997; Gabrielse et al., 2012; Sergeev et al., 2014). The electron velocity fluctuations ( $V_{Elc}$ , Figure 1h) differ from  $V_{Ion}$  indicating Hall  $\mathbf{E}$  may be deflecting the ion flow.  $\mathbf{E}$  fluctuations (Figure 1i) are particularly intense. The plasma density (Figure 1j) changes in consort with the flow vortex in  $V_{Ion}$  (Figure 1g).  $T_i$  and  $T_e$  increase (Figure 1k). These features are characteristic of the turbulent BBF braking region.

Shortly after the fluctuations in  $\mathbf{B}$ ,  $V_{Ion}$ ,  $V_{Elc}$ , and  $\mathbf{E}$  subside (~21:21 UT), the MMS satellites enter the radiation belt. Starting at ~21:22 UT, the intensity of energetic ion and electron fluxes

gradually increases whereas the fluctuations decrease.  $T_i$  and  $T_e$  also decrease. These observations insinuate that the BBF penetrated at least to the outer edge of the radiation belt.

One of the most important questions about this event is if and how the intense, turbulent  $\mathbf{E}$  locally energizes electrons and ions. As such, the nature of the turbulence and the properties of  $\mathbf{E}$  deserve further investigation. Figure 1L displays the frequency-domain power spectral density (PSD) of  $\mathbf{B}$  and  $\mathbf{E}$  in the BBF braking region. The black circles represent the measured PSDs. The light blue lines refer to the inertial region ( $f < \sim 0.4$  Hz) with previously measured spectral indices ( $\alpha$ ) of turbulent BBFs. The red and green lines are fits. These PSDs of  $\mathbf{B}$  and  $\mathbf{E}$  are remarkably similar to other identified turbulent events in the Earth's magnetotail (Ergun et al., 2015; 2018; 2020a,b). The spectral index of  $\mathbf{B}$  in the inertial region ( $f < \sim 0.4$  Hz) is consistent with  $-5/3$ ; the short period makes a fit uncertain. Mean plasma parameters, tabulated in Figure 1m, are such that the ion skin depth ( $d_i$ ) is greater than the ion gyroradius ( $\rho_i$ ) due to  $\sim 110$  nT background  $\mathbf{B}$ . We presume that the spectral break ( $\sim 0.4$  Hz) is near a region where the wavevector ( $\mathbf{k}$ ) is such that  $|\mathbf{k}|d_i \sim 1$ . The  $\mathbf{E}$  PSD at the lowest frequencies ( $< \sim 0.4$  Hz) is consistent with a shallow index previously observed ( $\alpha = -1.25$ ). The electrostatic or Hall region (Franci et al., 2015) of the  $\mathbf{E}$  PSD is between  $\sim 0.4$  Hz and  $\sim 40$  Hz with  $\alpha \sim -0.77$  (red line in Figure 1L). At higher frequencies, the  $\mathbf{E}$  PSD steeply declines.

From the measured PSD ( $P_E$ ), one can estimate the ion heating rate to be (Chang et al., 1986):

$$\dot{W}_i = \frac{e^2}{2m_i} \eta_L P_E(f_{ci}) \quad 1$$

Here,  $e$  is the fundamental charge,  $m_i$  is the ion mass, and  $\eta_L$  ( $\sim 1/2$ ) is the fraction of  $P_E$  that is left-hand polarized. Since  $P_E(f_{ci}) \sim 10 \text{ mV}^2 \text{ m}^{-2} \text{ Hz}^{-1}$  (Figure 1L),  $\dot{W}_i$  is estimated to be  $250 \text{ eV s}^{-1}$ ,



which is sufficient to explain the observed values of  $T_i$ . The development of the energetic ions requires a much more involved analysis and is reserved for a later study.

To the contrary, there is little power at  $f \geq f_{ce}$  (Figure 1L) and  $E_{\parallel}$  is small (written on plot) which, at first glance, suggests that electron energization should be negligible. Perpendicular energization requires circumvention of the first adiabatic invariant ( $\mu = p_{\perp}^2/2\gamma m_o B$ ). However, energization can occur if the correlation length scale ( $d_{corr}$ ) in the  $\mathbf{E}$  turbulence is sufficiently small. If an electron's parallel velocity is such that  $d_{corr\parallel}/v_{\parallel} < 1/f_{ce}$  it experiences changes in  $\mathbf{E}$  in less than  $1/f_{ce}$  (in its frame) and therefore can be energized perpendicular to  $\mathbf{B}$  (Ergun et al., 2020a,b). Furthermore, if an electron's gyroradius is such that  $\rho_e \geq d_{corr\perp}$ , it can experience enhanced parallel energization, perpendicular energization, and pitch-angle scattering.

Figures 1n, 1o, and 1p investigate the correlation length of  $\mathbf{E}$  beginning with the frequency range below  $f_{ci}$ , which is of interest for studying ion energization. The MMS spacecraft are separated from  $\sim 39$  to  $\sim 123$  km (Figure 1n). Figure 1o displays the correlation of  $\mathbf{E}$  filtered to DC to  $\sim 1.6$  Hz between each spacecraft pair. Each of the  $\mathbf{E}$  components is separately correlated then averaged. The measured correlations support an exponential with a correlation distance of  $\sim 140 \pm 50$  km, which lies between  $\rho_i$  (thermal average) and  $d_i$ , as expected in a turbulent plasma.

The correlation is repeated for the frequency range of  $\sim 1.6$  to  $\sim 100$  Hz (Figure 1p) in which the  $\mathbf{E}$  spectrum has a shallow slope (Figure 1L) and energization of electrons is expected to be governed. In this plot, correlations are performed over ten, one-minute intervals for each component of  $\mathbf{E}$  resulting in 30 individual correlations then averaged. Correlations using time lags, different periods, and separation of  $\mathbf{E}_{\perp}$  and  $E_{\parallel}$  unanimously indicate that  $\mathbf{E}$  is uncorrelated ( $< 0.05$ ) at the minimum separation of 39 km. This separation is primarily perpendicular to  $\mathbf{B}$ . This result suggests that  $d_{corr} < 10$  km (Figure 1p), which is consistent with  $d_e \sim 6$  km and

thermal  $\rho_e \sim 820$  m. Since  $\langle E_{\perp} \rangle_{RMS} \cong 7 \langle E_{\parallel} \rangle_{RMS}$ , the constraint on  $d_{corr}$  is likely that of  $d_{corr\perp}$ .

Furthermore, even though  $\partial \mathbf{B} / \partial t$  is visible (Figure 1b),  $|\nabla \times \mathbf{E}| \ll \langle \mathbf{E} \rangle_{RMS} / d_{corr}$ , so  $\mathbf{E}$  is

primarily electrostatic in this higher-frequency range (Figure 1L). Using  $\nabla \times \mathbf{E} \approx 0$ ,

$\langle E_{\parallel} \rangle_{RMS} / d_{corr\perp} \approx \langle E_{\perp} \rangle_{RMS} / d_{corr\parallel}$ , which implies  $d_{corr\parallel}$  is  $\sim 7 d_{corr\perp}$ .

### 3. Electron Energization and Test-Particle Simulations

In a magnetized plasma, parallel and perpendicular energization are distinct and quite complex. Energizing by  $E_{\parallel}$  can be amplified if  $\rho_e \geq d_{corr\perp}$ , which causes an electron's orbit to transit regions of uncorrelated  $E_{\parallel}$ . Perpendicular energization is often hindered since  $\mu$  is strongly conserved. An impulse from  $\mathbf{E}_{\perp}$  that endures for more than one gyroperiod is ineffective at energizing. However, if  $\rho_e \geq d_{corr\perp}$  or  $d_{corr\parallel} / v_{\parallel} < 1 / f_{ce}$ , an electron can experience impulses on time scales less than  $1 / f_{ce}$ . Since  $\rho_e = v_{\perp} / \omega_{ce}$ , these conditions can be expressed as:

$$v_{\parallel} \geq d_{corr\parallel} f_{ce} \text{ or } v_{\perp} \geq d_{corr\perp} \omega_{ce} \quad 2$$

In a turbulent environment, it is not unusual that  $d_{corr\perp} \approx d_e = c / \omega_{pe}$  so the condition for “full energization” (breaking of  $\mu$ ) can be estimated as:

$$\frac{p_{\perp}}{m_0 c} \geq \frac{\omega_{ce0}}{\omega_{pe}} \text{ or } \frac{p_{\parallel}}{m_0 c} \geq \frac{\omega_{ce0}}{\omega_{pe}} R_{corr} \text{ where } R_{corr} = \left( \frac{d_{corr\parallel}}{2\pi d_{corr\perp}} \right) \quad 3$$

Here,  $m_0$  is the electron rest mass and  $\omega_{ce0}$  represents the rest-mass electron cyclotron frequency.

$R_{corr}$ , a weighted parallel to perpendicular correlation ratio, is approximately unity in the observed event. The conditions in Equation (3) favor higher-energy particles and therefore

support acceleration. At the location of the MMS satellites,  $\omega_{ce0}/\omega_{pe} \sim 0.4$ , so only electrons with energies greater than  $\sim 40$  keV are expected to experience full energization from  $\mathbf{E}$ .

In a global-scale picture, electrons are free to travel along one of Earth's magnetic field lines and visit a range of values of  $|\mathbf{B}|$ , so  $\omega_{ce0}/\omega_{pe}$  also has an appreciable range since the plasma density remains relatively constant when far from Earth. MMS's location is at L-shell of  $\sim 8$ , which implies that lowest  $|\mathbf{B}|$  is  $\sim 60$  nT near the equator with  $\omega_{ce0}/\omega_{pe} \sim 0.21$ . There, electrons with energies  $> \sim 9$  keV meet the conditions for full energization (Equation 3). As a result, nowhere along the field line do core electrons ( $\sim 1.7$  keV) experience full energization. Nearer to Earth,  $\omega_{ce0}/\omega_{pe} > 1$  so only high- $\gamma$  electrons receive full energization.

To test this idea further, we perform a quasi-1D test-particle simulation of electrons along a  $L = 8$  field line (Figures 2a and 2b). The simulation code has modifications from a previously described version (Ergun et al., 2020b). The simulation domain ( $Z$ ) is 3D ( $20 R_E \times 36 d_e \times 36 d_e$ ), which is a long, narrow box. Electron velocities are tracked in 3D. The perpendicular dimensions are periodic; electrons can travel along  $\mathbf{B}$ , orbit  $\mathbf{B}$ , magnetically mirror, and receive impulses from  $\mathbf{E}$ , but cannot carry out curvature or  $\nabla_{\perp} B$  drifts (discussed later). Furthermore,  $E_{DC} = 0$  so there is no net drift.

The test-particle simulation is not self-consistent as it imposes  $\mathbf{E}$  and constant  $\mathbf{B}$ . A key feature of the simulation, however, is that  $\mathbf{E}$  is constructed to match the observed  $\langle \mathbf{E} \rangle_{RMS}$ , PDF (Figure 2c), spectrum (Figure 2d), and correlation lengths (Figure 1p). Since a realistic reproduction of  $\mathbf{E}$  is central to understanding local acceleration, we provide further detail (also see Figure 6 in Ergun et al., 2020b). Reconstructed  $\mathbf{E}$  is limited to the frequency range of  $\sim 1.6$  to  $\sim 100$  Hz, where most of the power lies. Since  $\mathbf{E}$  is primarily electrostatic, a scalar potential ( $\Phi$ ) is pseudo-randomly assigned so that the PDF of the reconstructed  $\mathbf{E}$  matches the observed PDF

and amplitude of  $\mathbf{E}$  (Figure 2c).  $\Phi$  is on a grid with perpendicular spacing proportional to  $d_{corr\perp}$ . Since  $d_{corr}$  is only constrained by observations,  $d_{corr\perp}$  is treated as a variable; the simulation is performed with  $d_{corr\perp}$  ranging from 2 km to 10 km. As discussed earlier, the electrostatic condition enforces  $d_{corr\parallel} = d_{corr\perp} \langle E_{\perp} \rangle_{RMS} / \langle E_{\parallel} \rangle_{RMS}$ . The resulting PSD versus  $|k|d_e$  ( $d_{corr\perp} = 8$  km) is plotted in Figure 2d. Mapping between  $|k|$  and  $f$  with a fixed velocity of  $2500 \text{ km s}^{-1}$  (nearly  $V_A$  the Alfvén velocity, Figure 1m) yields a good match to the measured  $\mathbf{E}$  PSD versus  $f$  (Figure 1L). As time advances,  $\Phi$  is regenerated every 10 ms to 500 ms, pseudo-randomly. This imposed time variation is consistent with observations and slow compared to  $1/f_{ce}$ . At the equator, for example, an electron undergoes 15 to 750 orbits before  $\Phi$  is altered.  $\langle \mathbf{E} \rangle_{RMS}$  is constant between  $Z = \pm 5 R_E$  (Figure 2b) but is reduced at larger values of  $Z$ .

The simulation is initiated with a  $T_e = 600 \text{ eV}$  Maxwellian distribution (see Figure 1k at 21:10 UT) with a constant density. Electrons then evolve in time under gyration, the magnetic mirror force, and  $\mathbf{E}$ . The  $\pm Z$  boundaries of the simulation are open. A particle that exits the domain is replaced by a randomly-generated thermal particle ( $T_e = 600 \text{ eV}$ ) at the boundary. More than 90% of particles initialized between  $Z = \pm 5 R_E$  remain in the simulation domain after 15 s due to the robust magnetic mirror. The simulation is tested for 50 s with  $\mathbf{E} = 0$  to assure conservation of energy. Tests also verify that energization is proportional  $\langle E^2 \rangle$ .

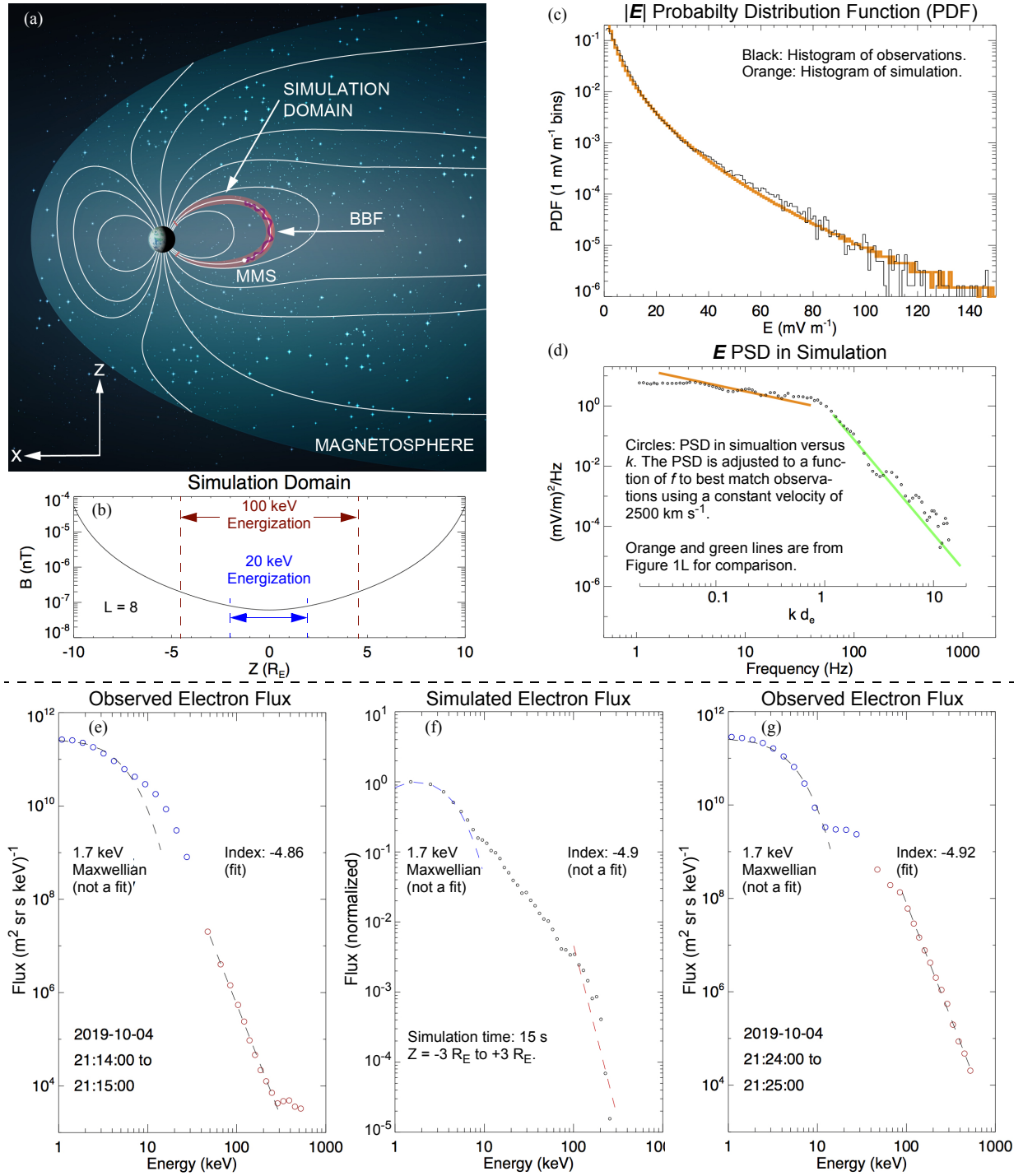


**Figure 2.** Details of and results from the test-particle simulation. (a) A cartoon depicting the simulation domain, which follows particles on a field line of  $L=8$ . (b)  $|B|$  in the simulation domain. (c) The PDF of  $|E|$  as observed (black) and in the simulation domain (orange). The

---

near-exact match is by design. (d) The PSD versus  $k$  in the simulation (circles) and the fits to the observed PSD versus  $f$  in Figure 1L (orange and green lines). Mapping between  $k$  and  $f$  using a velocity of  $2500 \text{ km s}^{-1}$  creates the best match. (e) The electron flux as observed during the turbulent event. (f) The electron flux from the test-particle simulation with  $d_{corr} = 8 \text{ km}$  at 15 s. (g) The electron flux as observed in the outer radiation belt.

---

After initiation, the simulation is advanced until electron distributions have an energy density similar to that observed. In the simulation, curvature and  $\nabla_{\perp} B$  drifts do not influence an electron's evolution. These drift speeds are proportional to energy ( $W$ ) and inversely proportional to  $|B|$ . A concern is that high-energy electrons drift relative to the thermal electrons on a closed field line and should have a different dwell times in the turbulent region. For example, a 100 keV electron trapped near the equator can drift relative to core electrons at a velocity of  $\sim 100 \text{ km s}^{-1}$ . If the scale size of a BBF is  $1 R_E$ , higher-energy ( $\sim 100 \text{ keV}$ ) electrons separate from the core in roughly 60 s. This interval is less than the observed duration of the turbulence ( $\sim 600 \text{ s}$ ; Figure 1) but greater than the simulation run times (15 s). As a result, curvature drifts and  $\nabla_{\perp} B$  drifts are inconsequential in the simulation, but should be significant in data interpretation.

Figures 2e-2g compare observed electron flux (intensity) with electron flux in the simulation. On the left (Figure 2e, black circles) is the observed electron flux as a function of energy compiled inside of the turbulent region. The time is written in the plot. In the center (Figure 2f) is a flux distribution ( $Z$  ranging from  $\pm 3 R_E$ ) from the simulation at  $t = 15 \text{ s}$  with  $d_{corr\perp} = \sim 8 \text{ km}$ . On the right (Figure 2g) is an observed flux distribution from the outer radiation belt. The shapes of the simulated and observed fluxes have several common characteristics. The core of the flux distributions have a similar  $T_e \sim 1.7 \text{ keV}$  (see dashed blue lines). Most noticeably, the observed

and simulation fluxes have a “shoulder” between  $\sim 10$  keV and  $\sim 100$  keV and a steep power-law tail (dashed lines at energies  $> 100$  keV. Setting  $d_{corr}$  to  $< 8$  km results in more core heating and faster energization.

The simulation’s  $\sim 15$  s run time to reach observed electron energy levels seems fast when compared to the duration of the BBF event (600 s), but is somewhat consistent with the time that curvature and  $\nabla_{\perp} B$  drifts separate electron populations. Furthermore, electron velocities (Figure 1h) and  $\mathbf{E}$  (Figure 1g) indicate substantial Hall fields (ions are decoupled). Electron flow speeds reach  $1000 \text{ km s}^{-1}$  and often differ from ion velocities by more than  $100 \text{ km s}^{-1}$ , which may limit an electron’s average dwell time in the region of turbulence to  $\sim 15$  s, which the simulation suggests.

There is one notable discrepancy between the simulation results and observations. The observed electron distributions are nearly isotropic (Figure 1k) whereas the simulated electron distributions have  $T_{e\perp} > T_{e\parallel}$ . This discrepancy likely results in part from the imposition of  $\langle E_{\perp} \rangle_{RMS} / \langle E_{\parallel} \rangle_{RMS} = 7$  over the entire simulation domain. This ratio is closer to 3 in other turbulent BBF events nearer to the equator (Ergun et al., 2015). Additionally, coherent waves such as Alfvén and whistler waves may act to pitch angle scatter electrons in the turbulent regions (e. g. Chaston et al, 2018).

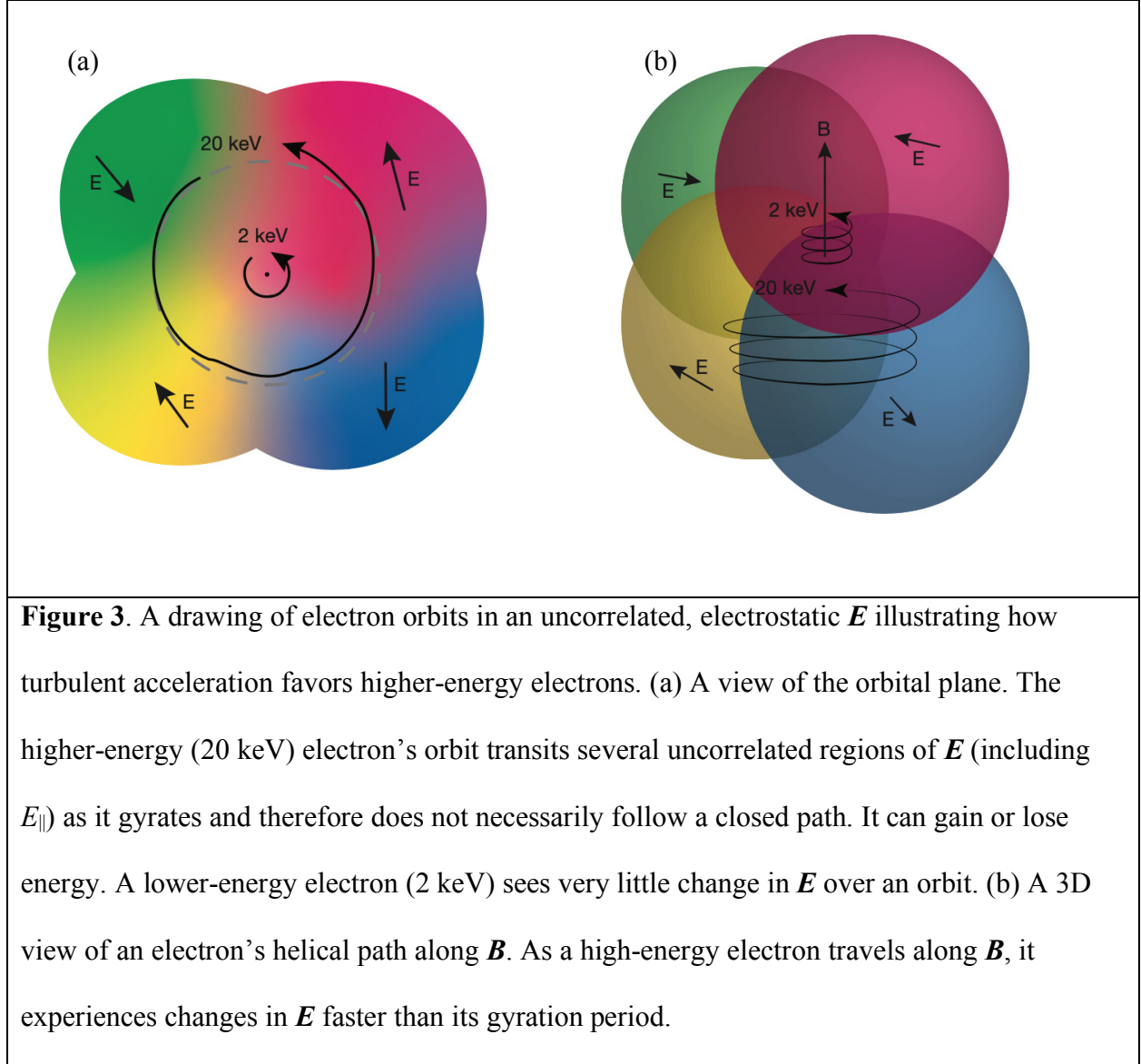
#### 4. Discussion and Conclusions

The MMS satellites detected a turbulent BBF braking region roughly  $7 R_E$  from Earth then entered the outer radiation belt. Of primary interest,  $T_i$  and  $T_e$  increase and high-energy ion and electron fluxes vary concurrently with  $\mathbf{E}$ ,  $\mathbf{B}$ , and  $V_{Ion}$  suggesting local energization and acceleration.

The properties of  $\mathbf{E}$  are investigated in detail including the spectra, correlation distance, PDF, and RMS amplitude. The four-spacecraft MMS mission constrained  $d_{corr}$  to be less than  $\sim 10$  km in the  $\sim 1.6$  to  $\sim 100$  Hz frequency range (Figure 1p). The fact that  $\mathbf{E}$  is uncorrelated at a relatively small separation is critical. Perpendicular energization requires violation of  $\mu$  conservation and there is little power in  $\mathbf{E}$  with  $f > f_{ce}$ . We hypothesized that if  $p_{\perp}/m_0c$  or  $p_{\parallel}/m_0c$  exceed  $\omega_{ce0}/\omega_{pe}$ , an electron experiences changes in  $\mathbf{E}$  faster than  $1/f_{ce}$ , which breaks conservation of  $\mu$ . This postulation also implies that the highest-energy electrons receive more energy than do the lower-energy electrons, which leads to the development a non-thermal shoulder and energetic tail in the electron distribution.

Figure 3 illustrates the basic idea of particle acceleration by turbulent, uncorrelated, electrostatic  $\mathbf{E}$ . In the plane of the gyration, a low-energy electron (2 keV in the drawing) experiences a nearly constant  $\mathbf{E}$  whereas a higher-energy electron (20 keV in the drawing) transits regions of changing  $\mathbf{E}$  during its gyration. Even though  $\mathbf{E}$  is primarily electrostatic, the particle does not necessarily return to the same location in the perpendicular plane (Figure 3a) or in the same location along  $\mathbf{B}$  (Figure 3b) and therefore can experience energy change. Either a high  $p_{\perp}$  or a high  $p_{\parallel}$  can lead to perpendicular energization. The time dependence of  $\mathbf{E}$ , albeit slow, is crucial in that an electron's energy gain is not limited to the largest variation in  $\Phi$ . Interestingly, a large  $p_{\perp}$  causes a particle to experience changing  $E_{\parallel}$ , which leads to parallel energization. A finite  $\nabla \times \mathbf{E}$  can enhance acceleration.





This hypothesis is tested with a quasi-1D test-particle simulation. Electrons are strongly magnetized and therefore well represented by a 1D simulation whereas ions require a much more complex investigation. A key aspect of the simulation is the careful reproduction of the observed  $\mathbf{E}$  including the  $d_{corr}$ , spectrum, parallel and perpendicular RMS power, and PDF. The salient result (Figures 2e-2g) is that the electron distributions develop an extended shoulder above  $\sim 10$  keV and an energetic tail. Despite its short-comings, (not self-consistent, RMS  $\mathbf{E}$  is the same at

all locations along  $\mathbf{B}$ , simulation distributions are not isotropic, drifts are not included), the simulation demonstrates the feasibility of local electron acceleration.

Analytically, one can estimate electron energization rates from random impulses via Equation 7 in Ergun et al, (2020b):

$$\dot{W} \approx \frac{e^2 \langle E^2 \rangle_{(W)} \langle \delta t \rangle_{(W)}}{2 W / c^2} \quad 4$$

where  $W = \gamma m_0 c^2$  and  $\langle E^2 \rangle_{(W)}$  represents the RMS  $\mathbf{E}$  experienced along an electron's helical path. Significantly,  $\langle E^2 \rangle_{(W)}$  is a function of  $W$  and strongly increases with  $W$ . The period of the impulses,  $\langle \delta t \rangle$ , is a fraction of the gyroperiod. For example, in Figure 3a,  $\langle \delta t \rangle_{(W)} \approx 1/(4f_{ce})$  for the 20 keV electron. From observations,  $\langle E^2 \rangle_{(W)} \approx 70 \text{ mV}^2 \text{ m}^{-2}$  and  $\langle \delta t \rangle \approx 8 \times 10^{-5} \text{ s}$ . A  $> \sim 20$  keV electron experiences  $\sim 500 \text{ eV/s}$  of energization on average, which agrees with the simulation. Core electrons ( $< 2 \text{ keV}$ ) experience a smaller  $\langle E^2 \rangle_{(W)}$  and receive significantly less energization. This analytical exercise illustrates why an electron distribution (Figure 2f) develops an extended shoulder above  $\sim 10 \text{ keV}$  (a  $\sim 10 \text{ keV}$  electron experiences full energization at the equator) while the core electrons are heated at a slower pace. For high- $\gamma$  electrons, we note that  $\langle \delta t \rangle_{(W)}$  is proportional to  $\gamma$ , so  $\dot{W}$  increases with energy.

Another interesting aspect unique to electrons trapped in a dipole field is illustrated in Figure 2b. The extent along  $\mathbf{B}$  in which an electron experiences full energization increases with an electron's energy (Equation 3). For example, a 100 keV electron is subject to full energization between  $Z = \pm 5 R_E$  where as a 20 keV electron only has full energization between  $Z = \pm 2 R_E$ . Consequently, higher-energy electrons again receive more energy, which further amplifies acceleration.

In conclusion, MMS observations of electron and ion acceleration from a BBF penetrating to  $\sim 7 R_E$  from Earth suggest local acceleration by turbulent  $\mathbf{E}$ . Electron acceleration is supported by test-particle simulation that used a realistic reproduction of the observed  $\mathbf{E}$ . The resulting enhanced shoulder and energetic tail in the electron distribution just outside of the radiation belts could be a significant supply of electrons for the outer radiation belt. If these electrons are adiabatically transported closer to Earth (higher  $|\mathbf{B}|$ , Gabrielse et al, 2012; Turner et al., 2015; 2016; Ukhorskiy et al., 2017; Sorathia et al., 2018; Turner et al., 2021), they can account for MeV electrons. A more far-reaching conclusion is that, since turbulence is pervasive in plasmas, it is likely a significant contributor to charged particle acceleration.

## **Acknowledgements**

Article is supported by NASA's MMS (NNG04EB99C) and THEMIS (NAS5-02099) missions. DLT received support from NASA grant 80NSSC19K0280, and DLT and MEU thank the International Space Sciences Institute for support. JES is supported by the Royal Society University Research Fellowship URF\R1\201286. All data used in this article are publicly available at <https://lasp.colorado.edu/mms/sdc/public/>.

## References

- Angelopoulos, V., W. Baumjohann, C. F. Kennel, F. V. Coroniti, M. G. Kivelson, R. Pellat, R. J. Walker, H. Lühr, and G. Paschmann (1992), Bursty bulk flows in the inner central plasma sheet, *J. Geophys. Res.*, 97(A4), 4027–4039, doi:10.1029/91JA02701
- Angelopoulos, V., Kennel, C. F., Coroniti, F. V., Pellat, R., Kivelson, M. G., Walker, R. J., ... Gosling, J. T. (1994). Statistical characteristics of bursty bulk flow events. *Journal of Geophysical Research*, 99(A11), 21,257– 21,280. <https://doi.org/10.1029/94JA01263>
- Baumjohann, W., G. Paschmann, and C. A. Cattell (1989), Average plasma properties in the central plasma sheet, *J. Geophys. Res.*, 94(A6), 6597–6606, doi:10.1029/JA094iA06p06597
- Birn, J., M. F. Thomsen, J. E. Borovsky, G. D. Reeves, D. J. McComas, and R. Belian (1997), Characteristic plasma properties during dispersionless substorm injections at geosynchronous orbit, *J. Geophys. Res.*, 102(A2), 2309– 2324, doi:10.1029/96JA02870.
- Burch, J. L., Moore, T. E., Torbert, R. B., & Giles, B. L. (2016). Magnetospheric Multiscale overview and science objectives. *Space Science Reviews*. <https://doi.org/10.1007/s11214-015-0164-9>
- Chang, T., Crew, G. B., Hershkowitz, N., Jasperse, J. R., Retterer, J. M., & Winningham, J. D. (1986). Transverse acceleration of oxygen ions by electromagnetic ion cyclotron resonance with broad band left-hand polarized waves. *Geophysical Research Letters*, 13(7), 636– 639. <https://doi.org/10.1029/GL013i007p00636>
- Chaston, C. C., Bonnell, J. W., Halford, A. J., Reeves, G. D., Baker, D. N., Kletzing, C. A., & Wygant, J. R. (2018). Pitch angle scattering and loss of radiation belt electrons in broadband electromagnetic waves. *Geophysical Research Letters*, 45, 9344– 9352. <https://doi.org/10.1029/2018GL079527>

- Dubyagin, S., V. Sergeev, S. Apatenkov, V. Angelopoulos, A. Runov, R. Nakamura, W. Baumjohann, J. McFadden, and D. Larson (2011), Can flow bursts penetrate into the inner magnetosphere?, *Geophys. Res. Lett.*, 38, L08102, doi:10.1029/2011GL047016.
- Ergun, R. E., K. A. Goodrich, J. E. Stawarz, L. Andersson, and V. Angelopoulos (2015), Large-amplitude electric fields associated with bursty bulk flow braking in the Earth's plasma sheet. *J. Geophys. Res. Space Physics*, 120, 1832–1844. doi: 10.1002/2014JA020165
- Ergun, R. E., Tucker, S., Westfall, J., Goodrich, K. A., Malaspina, D. M., Summers, D., ... Cully, C. M. (2016). The axial double probe and fields signal processing for the MMS mission. *Space Science Reviews*. <https://doi.org/10.1007/s11214-014-0115-x>
- Ergun, R. E., Goodrich, K. A., Wilder, F. D., Ahmadi, N., Holmes, J. C., Eriksson, S., Stawarz, J. E., Nakamura, R., Genestreti, K. J., Hesse, M., & Burch, J. L. (2018). Magnetic reconnection, turbulence, and particle acceleration: Observations in the Earth's magnetotail. *Geophysical Research Letters*, 45, 3338– 3347. <https://doi.org/10.1002/2018GL076993>
- Ergun, R. E., Ahmadi, N., Kromyda, L., Schwartz, S. J., Chasapis, A., Hoilijoki, S., Wilder, F. D., Stawarz, J. E., Goodrich, K. A., Turner, D. L., Cohen, I. J., Bingham, S. T., Holmes, J. C., Nakamura, R., Pucci, F., Torbert, R. B., Burch, J. L., Lindqvist, P. A., Strangeway, R. J., le Contel, O., & Giles, B. L. (2020a). Observations of particle acceleration in magnetic reconnection-driven turbulence. *The Astrophysical Journal*, 898(2), 154. <https://doi.org/10.3847/1538-4357/ab9ab6>
- Ergun, R. E., Ahmadi, N., Kromyda, L., Schwartz, S. J., Chasapis, A., Hoilijoki, S., et al. (2020b). Particle acceleration in strong turbulence in the Earth's magnetotail. *The Astrophysical Journal*, 898(15), 153. <https://doi.org/10.3847/1538-4357/ab9ab5>
- Franci, L., Landi, S., Matteini, L., Verdini, A., & Hellinger, P. (2015). High-resolution hybrid

- simulations of kinetic plasma turbulence at proton scales. *The Astrophysical Journal*, 812, 21.  
<https://doi.org/10.1088/0004-637X/812/1/21>
- Gabrielse, C., Angelopoulos, V., Runov, A., & Turner, D. L. (2012). The effects of transient, localized electric fields on equatorial electron acceleration and transport toward the inner magnetosphere. *Journal of Geophysical Research*, 117, A10213.  
<https://doi.org/10.1029/2012JA017873>
- LeContel, O., Leroy, P., Roux, A., Coillot, C., Alison, D., Bouabdellah, A., ... de la Porte, B. (2016). The Search-Coil Magnetometer for MMS. *Space Science Reviews*, 199, 257– 282.  
<https://doi.org/10.1007/s11214-014-0096-9>
- Lindqvist, P.-A. *et al.* (2016), The spin-plane double probe instrument for MMS, *Space Sci. Rev.* 199, 137-165, doi:10.1007/s11214-014-0116-9.
- Liu, J., Angelopoulos, V., Zhang, X.-J., Turner, D. L., Gabrielse, C., Runov, A., et al. (2016). Dipolarizing flux bundles in the cis-geosynchronous magnetosphere: Relationship between electric fields and energetic particle injections. *Journal of Geophysical Research: Space Physics*, 121(2), 1362– 1376. <https://doi.org/10.1002/2015JA021691>
- Nakamura, R., W. Baumjohann, R. Schvdel, M. Brittnacher, V. A. Sergeev, M. Kubyshkina, T. Mukai, and K. Liou (2001), Earthward flow bursts, auroral streamers, and small expansions, *J. Geophys. Res.*, 106, 10,791– 10,802, doi:10.1029/2000JA000306
- Nakamura, R., et al. (2009), Evolution of dipolarization in the near-Earth current sheet induced by Earthward rapid flux transport, *Ann. Geophys.*, 27, 1743– 1754
- Mauk, B. H., et al. (2016), The energetic Particle Detector (EPD) investigation and the Energetic Ion Spectrometer (EIS) for the Magnetospheric Multiscale (MMS) mission, *Space Sci. Rev.*, 199(1), 471–514, doi:10.1007/s11214-014-0055-5

- Ohtani, S., H. J. Singer, and T. Mukai (2006), Effects of the fast plasma sheet flow on the geosynchronous magnetic configuration: Geotail and GOES coordinated study, *J. Geophys. Res.*, 111, A01204, doi:10.1029/2005JA011383
- Pollock, C., Moore, T., Jacques, A., Burch, J., Gliese, U., Saito, Y., ... Zeuch, M. (2016). Fast Plasma Investigation for Magnetospheric Multiscale. *Space Science Reviews*, 199, 331– 406. <https://doi.org/10.1007/s11214-016-0245-4>
- Runov, A., V. Angelopoulos, M. I. Sitnov, V. A. Sergeev, J. Bonnell, J. P. McFadden, D. Larson, K.-H. Glassmeier, and U. Auster (2009), THEMIS observations of an earthward-propagating dipolarization front, *Geophys. Res. Lett.*, 36, L14106, doi:10.1029/2009GL038980
- Runov, A., V. Angelopoulos, X.-Z. Zhou, X.-J. Zhang, S. Li, F. Plaschke, and J. Bonnell (2011), A THEMIS multicase study of dipolarization fronts in the magnetotail plasma sheet, *J. Geophys. Res.*, 116, A05216, doi:10.1029/2010JA016316
- Russell, C. T., Anderson, B. J., Baumjohann, W., Bromund, K. R., Dearborn, D., Fischer, D., ... Richter, I. (2016). The Magnetospheric Multiscale magnetometers. *Space Science Reviews*, 199, 189– 256. <https://doi.org/10.1007/s11214-014-0057-3>
- Sergeev, V. A., K. Liou, C.-I. Meng, P. T. Newell, M. Brittnacher, G. Parks, and G. D. Reeves (1999), Development of auroral streamers in association with localized impulsive injections to the inner magnetotail, *Geophys. Res. Lett.*, 26(3), 417– 420, doi:10.1029/1998GL900311
- Sergeev, V. A., et al. (2000), Multiple-spacecraft observation of a narrow transient plasma jet in the Earth's plasma sheet, *Geophys. Res. Lett.*, 27(6), 851– 854, doi:10.1029/1999GL010729
- Sergeev, V. A., Chernyaev, I. A., Dubyagin, S. V., Miyashita, Y., Angelopoulos, V., Boakes, P. D., Nakamura, R., and Henderson, M. G. (2012), Energetic particle injections to geostationary orbit: Relationship to flow bursts and magnetospheric state, *J. Geophys. Res.*, 117, A10207,

doi:10.1029/2012JA017773.

Sergeev, V. A., Chernyaev, I. A., Angelopoulos, V., Runov, A. V., & Nakamura, R. (2014).

Stopping flow bursts and their role in the generation of the substorm current wedge.

*Geophysical Research Letters*, 41, 1106– 1112. <https://doi.org/10.1002/2014GL059309>

Sitnov, M. I., Swisdak, M., & Divin, A. V. (2009). Dipolarization fronts as a signature of

transient reconnection in the magnetotail. *Journal of Geophysical Research*, 114, A04202.

<https://doi.org/10.1029/2008JA013980>

Sorathia, K. A., Ukhorskiy, A. Y., Merkin, V. G., Fennell, J. F., & Claudepierre, S. G. (2018).

Modeling the depletion and recovery of the outer radiation belt during a geomagnetic storm:

Combined MHD and test particle simulations. *Journal of Geophysical Research: Space*

*Physics*, 123(7), 5590– 5609. <https://doi.org/10.1029/2018JA025506>

Stawarz, J. E., Ergun, R. E., & Goodrich, K. A. (2015). Generation of high-frequency electric

field activity by turbulence in the Earth's magnetotail. *Journal of Geophysical Research:*

*Space Physics*, 120, 1845– 1866. <https://doi.org/10.1002/2014JA020166>

Takada, T., R. Nakamura, W. Baumjohann, Y. Asano, M. Volwerk, T. L. Zhang, B. Klecker, H.

Réme, E. A. Lucek, and C. Carr (2006), Do BBFs contribute to inner magnetosphere

dipolarizations: Concurrent Cluster and Double Star observations, *Geophys. Res. Lett.*, 33,

L21109, doi:10.1029/2006GL027440

Torbert, R. B., Russell, C. T., Magnes, W., Ergun, R. E., Lindqvist, P.-A., LeContel, O., ...

Lappalainen, K. (2016). The FIELDS instrument suite on MMS: Scientific objectives,

measurements, and data products. *Space Science Reviews*, 199, 105– 135.

<https://doi.org/10.1007/s11214-014-0109-8>

Turner, D. L., Claudepierre, S. G., Fennell, J. F., O'Brien, T. P., Blake, J. B., Lemon, C.,



- Gkioulidou, M., Takahashi, K., Reeves, G. D., Thaller, S., Breneman, A., Wygant, J. R., Li, W., Runov, A., and Angelopoulos, V. (2015), Energetic electron injections deep into the inner magnetosphere associated with substorm activity. *Geophys. Res. Lett.*, 42, 2079– 2087. doi: 10.1002/2015GL063225
- Turner, D. L., Fennell, J. F., Blake, J. B., Clemmons, J. H., Mauk, B. H., Cohen, I. J., ... Burch, J. L. (2016). Energy limits of electron acceleration in the plasma sheet during substorms: A case study with the Magnetospheric Multiscale (MMS) mission. *Geophysical Research Letters*, 43, 7785– 7794. <https://doi.org/10.1002/2016GL069691>
- Turner D. L., Cohen I. J., Michael A., Sorathia K., Merkin S., Mauk B. H., Ukhorskiy S., et al., 2021, Can Earth's Magnetotail Plasma Sheet Produce a Source of Relativistic Electrons for the Radiation Belts? *Geophysical Research Letters*, 45, e95495. doi:10.1029/2021GL095495
- Ukhorskiy, A. Y., Sitnov, M. I., Merkin, V. G., Gkioulidou, M., & Mitchell, D. G. (2017). Ion acceleration at dipolarization fronts in the inner magnetosphere. *Journal of Geophysical Research: Space Physics*, 122, 3040– 3054. <https://doi.org/10.1002/2016JA023304>
- Usanova, M. E. and Ergun R. E. (2022). Electron Energization by Turbulent Electric Fields: A Possible Source of the Outer Radiation Belt (preprint). <https://essoar.org> (2022), doi: 10.1002/essoar.10510040.1

## Figure Captions

**Figure 1.** MMS1 observations of a BBF penetrating close to the outer radiation belt. The horizontal axis on the right column is 50 minutes in time. Vectors are in GSE coordinates; colors represent components as marked on the right of a panel. (a)  $\mathbf{B}$  at 62.5 ms resolution. The black trace is  $|\mathbf{B}|$ . (b)  $\mathbf{B}$  detrended by 10 s. (c) Ion flux as a function of energy (vertical axis) from 70 to 600 keV. These data are from all four MMS spacecraft. (d) Differential ion energy flux as a function of energy from 3 eV to 25 keV. (e) Electron flux from 60 to 500 keV. (f) Differential electron energy flux 6 eV to 25 keV. (g)  $V_{Ion}$  at 4.5 s resolution. (h)  $V_{Elc}$  at 4.5 s resolution smoothed over 13.5 s. (i)  $\mathbf{E}$  at 31.25 ms resolution. (j) Electron density at 4.5 s resolution. (k)  $T_i$  and  $T_e$  at 4.5 s resolution. (L) The PSD of  $\mathbf{B}$  and  $\mathbf{E}$  versus frequency. (m) Average plasma conditions. (n) The relative positions of the MMS spacecraft. (o) The cross-correlation of  $\mathbf{E}$  between the MMS spacecraft plotted as a function of separation.  $\mathbf{E}$  is filtered from DC to 1.6 Hz. (p) The cross-correlation of  $\mathbf{E}$  filtered from 1.6 Hz to 100 Hz.

**Figure 2.** Details of and results from the test-particle simulation. (a) A cartoon depicting the simulation domain, which follows particles on a field line of  $L=8$ . (b)  $|\mathbf{B}|$  in the simulation domain. (c) The PDF of  $|\mathbf{E}|$  as observed (black) and in the simulation domain (orange). The near-exact match is by design. (d) The PSD versus  $k$  in the simulation (circles) and the fits to the observed PSD versus  $f$  in Figure 1L (orange and green lines). Mapping between  $k$  and  $f$  using a velocity of  $2500 \text{ km s}^{-1}$  creates the best match. (e) Electron flux as observed during the turbulent event. (f) Electron flux from the test-particle simulation with  $d_{corr} = 8 \text{ km}$  at 15 s. (g) Electron flux as observed in the outer radiation belt.

**Figure 3.** A drawing of electron orbits in an uncorrelated, electrostatic  $\mathbf{E}$  illustrating how turbulent acceleration favors higher-energy electrons. (a) A view of the orbital plane. The higher-energy (20 keV) electron's orbit transits several uncorrelated regions of  $\mathbf{E}$  (including  $E_{\parallel}$ ) as it gyrates and therefore does not follow a closed path. It can gain or lose energy. A lower-energy electron (2 keV) sees little change in  $\mathbf{E}$  over an orbit. (b) A 3D view of an electron's helical path along  $\mathbf{B}$ . As a high-energy electron travels along  $\mathbf{B}$ , it experiences changes in  $\mathbf{E}$  faster than its gyration period.